MARCH 21 2025

Measuring vessel source level in shallow water using the smoothed semi-coherent image method

Roberto Yubero ; Christ A. F. de Jong ; Michael A. Ainslie ; Alexander O. MacGillivray ; Lian Wang

J. Acoust. Soc. Am. 157, 1938–1954 (2025)
https://doi.org/10.1121/10.0036140

JASA ARTICLE

Measuring vessel source level in shallow water using the smoothed semi-coherent image method

Roberto Yubero,[1,a] Christ A. F. de Jong,[2] Michael A. Ainslie,[3] Alexander O. MacGillivray,[4] and Lian Wang[5]

[1]*TSI, Madrid, Spain*

[2]*TNO, The Hague, Netherlands*

[3]*JASCO Applied Sciences (Deutschland) GmbH, Schwentinental, Germany*

[4]*JASCO Applied Sciences (Canada) Ltd., Victoria, Canada*

[5]*NPL, Teddington, United Kingdom*

ABSTRACT:

Standardizing the process for measuring underwater sound generated by ships in shallow waters is a complex challenge currently under development. Recent progress has enabled the development of analytical formulations to represent propagation conditions underwater using propagation loss (PL) approximations, which are employed to derive the source level (SL) from ship sound pressure level (SPL) measurements. Underwater radiated noise (URN) tests conducted in the SATURN project enabled a detailed evaluation of the seabed critical angle (SCA) method, recommended by an early draft of the ongoing ISO 17208-3 standard, identifying a general underestimation of SL above ~500 Hz compared to measurements under equivalent operating conditions in deep water, as described by ISO 17208-1. This article presents an alternative smoothed semi-coherent image (SSCI) method for calculating PL (and hence SL) and assesses the method's performance through analytical and empirical scenarios (including recordings of three different instrumentation deployment strategies at four distinct depths and four test distances). The SSCI method enhances accuracy over a broad frequency range while maintaining the general robustness, with a formulation that also seeks to preserve the simplicity of the SCA approach.

 https://doi.org/10.1121/10.0036140

(Received 15 October 2024; revised 21 January 2025; accepted 22 February 2025; published online 21 March 2025)

[Editor: James F. Lynch] Pages: 1938–1954

I. INTRODUCTION

For almost a decade, there has been an international standard for measuring underwater radiated noise (URN) from ships in deep water (ISO 17208-1:2016, 2016), which was based on a previous standard from the American National Standards Institute (Bahtiarian, 2009; Blaeser and Struck, 2019). Under the conditions described in ISO 17208-1, the sound interactions with the seabed have a negligible impact, so this standard allows for accurate characterization of underwater sound from vessels using a simple logarithmic distance correction [$20 \cdot \log_{10}(R)$]. The resulting metric, known as radiated noise level (RNL), is intended to be used to show compliance with URN noise criteria or to compare ships. In 2019, the second part of the standard was published (ISO 17208-2:2019, 2019), enabling the conversion of RNL to the source level (SL) metric. This metric is intended to be used with acoustic propagation models, which are needed for applications such as underwater soundscape modelling. However, the requirement for measuring in deep water (typically at depths greater than the maximum of 1.5 times the ship length and 150 m) is often impractical. In 2021, ISO began developing the first international standard for measuring ship noise in shallow waters. A draft version of the standard [draft international standard (DIS) ISO/DIS 17208-3 (2023)] was available for this study. This DIS may differ from the final published standard. The details of the procedures tested in this study are presented in this paper. The direct output metric is SL, enabling the assessment of a ship's underwater noise footprint via acoustic models (using SL), which can be analytically converted to RNL for comparing ship signatures.

The SATURN project (SATURN, 2020) focuses on researching solutions to the problem of URN caused by shipping. Specific project tests focused on characterizing the URN for one vessel using different measurement procedures, comparing the results, and demonstrating the need for standardized methods, as previously identified by Ainslie *et al.* (2022) and Ainslie and Wood (2022). The SATURN test campaign results revealed differences of up to 12 dB in the URN levels obtained using different methods, despite being from the same ship under identical operational conditions (Yubero *et al.*, 2023). Additionally, this campaign facilitated measurements based on a draft of the shallow

[a]Email: roberto.yubero@tsisl.es

https://doi.org/10.1121/10.0036140

water standard (ISO/DIS 17208-3, 2023), enabling the use of various hydrophone setups, including vertical arrays, horizontal arrays, and single hydrophone deployments. These tests were conducted in November 2022 over a nine-day test campaign, with data from seven days of measurements used in this study. Measurements were taken at various water depths (40, 50, 80, and 200 m) and closest approach distances (50, 100, 150, and 200 m), while maintaining consistent operational conditions for the studied ship. All measurements included in the analysis complied with the draft standard's restrictions.

Calculation of SL from sound pressure level (SPL) measurements in shallow waters involves a correction for propagation loss (PL) (ISO 18405:2017, 2017). Quantifying PL is a complex undertaking that has historically been addressed using various propagation models or combinations of models (Wang *et al.*, 2014), which require advanced knowledge of the underwater modelling field (Etter, 2013; Jensen *et al.*, 2011). Moreover, comparative studies have shown that the complexity of these models does not always ensure their robustness (Lagrois *et al.*, 2024), as uncertainties in input parameters (e.g., precise seabed composition) can lead to significant deviations in computed PL (MacGillivray *et al.*, 2023). Due to the challenges mentioned (usage difficulty and robustness), ISO/DIS 17208-3 (2023) has focused on using analytical methods for PL computation rather than numerical propagation models.

The draft shallow water standard tested in the SATURN project specified the seabed critical angle (SCA) method for calculating PL (Sec. II A). The test results using this method showed a general underestimation of SLs at frequencies above ~500 Hz by approximately 2.5 dB when comparing shallow water results with those from deep water (Yubero *et al.*, 2023). This deviation was further studied by members of the working group developing the standard ISO/TC 43/SC 3/WG 1 (2011), resulting in approximations aimed at improving the accuracy of the SCA method, yielding an enhanced version known as SCA+ (Ainslie *et al.*, 2024b). The improved method demonstrated greater accuracy in most frequency bands, but it compromised robustness at some frequencies, as the PL lacked the smoothing effect provided by the original SCA method, which had proven to be a good fit for on-site measurements.

The smoothed semi-coherent image (SSCI) method, developed and described in this study, aims to maintain the improved accuracy of SCA+ at mid and high frequencies without sacrificing precision at low frequencies. This article explains its derivation, analyzes its accuracy across various synthetic scenarios by comparing the results with a complex yet proven numerical propagation model [OASES; see Schmidt and Jensen (1985)], and concludes by evaluating its performance in real test cases. The method was applied to data from the SATURN project, and its evaluation was complemented by reanalyzing measurements from the MMP2 project (MacGillivray *et al.*, 2022).

This article is accompanied by supplementary documentation, including a spreadsheet that computes PL for the SSCI method, a complete mathematical derivation of the SSCI method in a separate document, and measured SPL from the SATURN project used for the comparisons from Sec. V F.

General acoustical terminology follows ISO 80000-8:2020 (2020). Underwater acoustical terminology follows ISO 18405:2017 (2017), supplemented where needed by SATURN deliverable D2.3 (Ainslie *et al.*, 2024a).

II. SL CALCULATION

For the purpose of measuring its SL L_S, a vessel is characterized as an omnidirectional point source at nominal source depth d_s below the water surface. Hydrophone measurements are taken at a horizontal distance, the closest point of approach (CPA) distance (d_{CPA}), and at depth(s) d_h below the surface (see Fig. 1). The paths shown in Fig. 1 account for the combined sound from the source and its surface image.

The SPL L_p measured by the hydrophone is combined with a calculated PL, N_{PL}, to determine the SL:

$$L_S = L_p + N_{PL}. \tag{1}$$

The PL N_{PL} is equal to 10 $\log_{10}(F_p{}^{-1}/1\ \mathrm{m}^2)$ dB, where F_P is the propagation factor (ISO 18405:2017, 2017).

Following the "image method" approximation for a flat waveguide [see, e.g., Jensen *et al.* (2011)], the various reflections at sea surface and bottom are represented by mirror images. The contributions of the sound paths are added to calculate the resulting propagation factor. Coherent addition requires a numerical algorithm involving complex numbers. Various proposals have been made for a simpler and more robust approach for practical application in the measurement standard. The semi-coherent formula (SCF), proposed by Ainslie and Wood (2022), combines a coherent sum over the direct and the first surface reflected sound paths from the source to the hydrophone with an incoherent sum over a truncated series of bottom and surface reflections of the sound path from this initial image pair. Various

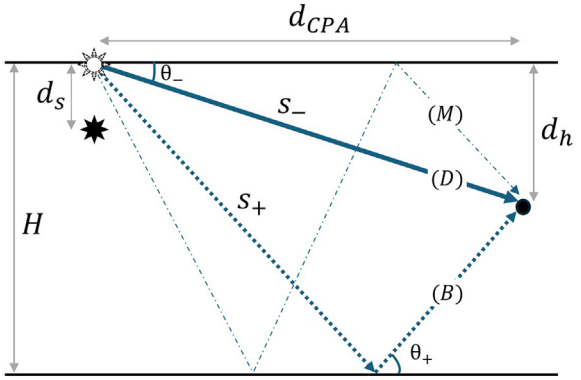

FIG. 1. Geometry for the contributions from direct (D), bottom-reflected (B), and multiple reflected (M) paths from the dipole at the water surface (hollow star) formed by the source (solid star) and its surface image (not shown). Adapted from Ainslie and Wood (2022) and Ainslie *et al.* (2024b).

alternatives have been proposed and tested against measurements by MacGillivray *et al.* (2023). Based on this study, ISO/DIS 17208-3 (2023) proposed the SCA formula as the preferred method for calculating PL. The SCA and SCF formulas were compared for a test case in Ainslie *et al.* (2024b). This comparison showed that the PL calculated by the SCA formula was 1–2 dB lower than the PL calculated by the SCF at frequencies above about 1 kHz. This difference was further investigated by Ainslie *et al.* (2024b), leading to the proposal for an enhanced SCA formula (SCA+). This eliminated the 1–2 dB underestimation of SL at high frequency when using SCA. However, SCA+ was found to be less robust than SCA. Further investigations led to the improved SSCI method formula proposed below.

A. SCA formula

The SCA method provides a simple formula for the propagation factor F, as introduced by MacGillivray *et al.* (2023). It combines the coherent sum of the direct and surface reflected sound paths with a contribution of the bottom reflections, depending on the seabed critical angle ψ_c,

$$\psi_\mathrm{c} = \cos^{-1}(c_\mathrm{w}/c_\mathrm{b}), \tag{2}$$

where c_w is the speed of sound in water and c_b the speed of sound in the seabed. The method is only applicable when $c_b > c_w$.

The SCA formula is

$$N_\mathrm{PL,SCA} = -10\lg\left(\sigma_1 + \frac{\psi_\mathrm{c} r_\mathrm{h}}{H}\sigma_2\right)\frac{r_0^2}{r_\mathrm{h}^2}\,\mathrm{dB}, \tag{3}$$

$$\sigma_1 = \frac{1}{2} + \frac{1}{4(k_\mathrm{w} d_s)^2 \sin^2\theta_i}\Bigg)^{-1}, \tag{4}$$

$$\sigma_2 = \frac{1}{2} + \frac{3}{4(k_\mathrm{w} d_s)^2 \sin^2\psi_\mathrm{c}}\Bigg)^{-1}, \tag{5}$$

where $r_0 = 1$ m is the reference distance, $k_\mathrm{w} = 2\pi f/\mathrm{c}_w$ is the wavenumber in water, H is the water depth, $r_h^2 = d_\mathrm{CPA}^2 + d_h^2$ is the slant range, d_h is the hydrophone depth below the water surface and $\theta_h = \tan^{-1}(d_h/d_\mathrm{CPA})$ the observation angle (s_-, d_h, and θ_-, respectively, in Fig. 1).

B. SSCI method

A SSCI method is proposed that is demonstrated here to be as robust as the SCA method but eliminates the observed bias at high frequency. It is based on a re-evaluation of the approximations that led to the SCA formulas. The derivation starts from the semi-coherent sum (Ainslie and Wood, 2022) identifying three main contributions (Fig. 1),

(1) the direct path from the surface dipole (D), with path length s_- and path angle θ_-,
(2) the first seabed reflected path (B), with path length s_+ and path angle θ_+,
(3) multiple reflected paths (M), so that

$$F_\mathrm{P} \approx F_\mathrm{P,D} + F_\mathrm{P,B} + F_\mathrm{P,M}, \tag{6}$$

with

$$F_\mathrm{P,D} \approx 4\frac{\sin^2(k_\mathrm{w} d_\mathrm{s}\sin\theta_-)}{s_-^2}, \tag{7}$$

$$F_\mathrm{P,B} \approx 4\frac{R_P(\theta_+)\sin^2(k_\mathrm{w} d_\mathrm{s}\sin\theta_+)}{s_+^2}, \tag{8}$$

$$F_\mathrm{P,M} \approx 4\sum_{m=1}^{M}\frac{(R_\mathrm{P}(\theta_m))^m(1+R_\mathrm{P}(\theta_m))\sin^2(k_\mathrm{w} d_s\sin\theta_m)}{s_m^2}. \tag{9}$$

The power reflection coefficient of the seabed reflected paths $R_P(\theta)$ depends on the acoustic properties of seawater and seabed. The seawater is characterized as a uniform fluid with sound speed c_w and density ρ_w. Sound absorption in seawater is ignored because short distances and not very high frequencies are considered (see also Section L). The seabed is approximately described as a uniform fluid with sound speed c_b, density ρ_b, and absorption loss per wavelength β_b. The power reflection coefficient can be calculated using complex arithmetic (Ainslie, 2010),

$$R_P(\theta_+) = \left|\frac{\frac{wv}{(1+\mathrm{i}\varepsilon)}\sin\theta_+ - \sqrt{1-\frac{v^2}{(1+\mathrm{i}\varepsilon)^2}\cos^2\theta_+}}{\frac{wv}{(1+\mathrm{i}\varepsilon)}\sin\theta_+ + \sqrt{1-\frac{v^2}{(1+\mathrm{i}\varepsilon)^2}\cos^2\theta_+}}\right|^2, \tag{10}$$

with density ratio $w = \rho_b/\rho_w$, sound speed ratio $v = c_b/c_w$, and loss factor $\varepsilon = (ln10/40\pi)(\beta_\mathrm{b}/\mathrm{dB})$. It is assumed that the speed of sound in the seabed is greater than that in the seawater ($c_\mathrm{b} > c_\mathrm{w}$), so that sound reflection at the seabed depends on the seabed critical angle. Note that this approach may be generalized to a non-uniform seabed by varying the sound speed ratio with frequency, as in MacGillivray *et al.* (2023), to simulate a frequency-dependent critical angle (see Sec. VI).

As proposed for the SCA method (MacGillivray *et al.*, 2023), the sum over the multiple reflected paths is approximated by an integral over path angles, while assuming that the reflection coefficient equals 1 for path angles smaller than the seabed critical angle ($R_P(\theta_m < \psi_c) = 1$) and zero for greater path angles ($R_P(\theta_m > \psi_c) = 0$),

$$F_\mathrm{P,M} \approx 4\int_{\theta_\mathrm{min}}^{\psi_\mathrm{c}}\frac{\sin^2(k_\mathrm{w} d_\mathrm{s}\sin\theta)}{d_\mathrm{CPA} H}\,\mathrm{d}\theta, \tag{11}$$

https://doi.org/10.1121/10.0036140

with minimum ray angle ($\theta_{\min}$),

$$\theta_{\min} = \min\left(\psi_c, \operatorname{atan}\frac{2H}{d_{\mathrm{CPA}}}\right). \tag{12}$$

The simplification to the reflection coefficient leading to Eq. (11) is used for the evaluation of $F_{\mathrm{P,M}}$, while Eq. (10) is used for $F_{\mathrm{P,B}}$. Averaged in decidecade frequency bands, the resulting propagation factors are

$$F_{\mathrm{P,D,ddec}} \approx \frac{2}{s_-^2}\left(1 - \frac{\sin(2k_{\mathrm{hi}}d_s\sin\theta_-) - \sin(2k_{\mathrm{lo}}d_s\sin\theta_-)}{2(k_{\mathrm{hi}} - k_{\mathrm{lo}})d_s\sin\theta_-}\right), \tag{13}$$

$$F_{\mathrm{P,B,ddec}} \approx \frac{2R_P(\theta_+)}{s_+^2} \times \left(1 - \frac{\sin(2k_{\mathrm{hi}}d_s\sin\theta_+) - \sin(2k_{\mathrm{lo}}d_s\sin\theta_+)}{2(k_{\mathrm{hi}} - k_{\mathrm{lo}})d_s\sin\theta_+}\right), \tag{14}$$

$$F_{\mathrm{P,M,ddec}} \approx \frac{2}{d_{\mathrm{CPA}}H} \times \int_{\theta_{\min}}^{\psi_c}\left(1 - \frac{\sin(2k_{\mathrm{hi}}d_s\sin\theta) - \sin(2k_{\mathrm{lo}}d_s\sin\theta)}{2(k_{\mathrm{hi}} - k_{\mathrm{lo}})d_s\sin\theta}\right)\mathrm{d}\theta, \tag{15}$$

where k_c is the wavenumber k_w at the band centre frequency, the wavenumbers at the upper and lower decidecade band edge frequencies are $k_{\mathrm{hi}} = 10^{0.05}k_c$ and $k_{\mathrm{lo}} = 10^{-0.05}k_c$, and $R_P(\theta_+)$ is given by Eq. (10).

Approximate solutions to the above equations can be found for low frequencies (LF; $k_w d_s \ll 1$) and high frequencies (HF; $k_w d_s \gg 1$), respectively,

$$F_{\mathrm{P,D,ddec,LF}} \approx \xi\frac{(2k_c d_s\sin\theta_-)^2}{s_-^2}, \tag{16}$$

$$F_{\mathrm{P,B,ddec,LF}} \approx \xi R_{\mathrm{P}}(\theta_+)\frac{(2k_c d_s\sin\theta_+)^2}{s_+^2}, \tag{17}$$

$$F_{\mathrm{P,M,ddec,LF}} \approx \xi\frac{4}{3}\frac{(k_c d_s)^2}{d_{\mathrm{CPA}}H}\left({\psi_c}^2\sin\psi_c - \theta_{\min}^2\sin\theta_{\min}\right), \tag{18}$$

where

$$\xi = \frac{1}{3}\left(\left(\frac{k_{\mathrm{hi}}}{k_c}\right)^2 + \frac{k_{\mathrm{hi}}k_{\mathrm{lo}}}{k_c^2} + \left(\frac{k_{\mathrm{lo}}}{k_c}\right)^2\right) \approx 1.0178 \tag{19}$$

and

$$F_{\mathrm{P,D,ddec,HF}} \approx \frac{2}{s_-^2}, \tag{20}$$

$$F_{\mathrm{P,B,ddec,HF}} \approx R_{\mathrm{P}}(\theta_+)\frac{2}{s_+^2}, \tag{21}$$

$$F_{\mathrm{P,M,ddec,HF}} \approx \frac{2}{d_{\mathrm{CPA}}H}(\psi_c - \theta_{\min}). \tag{22}$$

Multiple reflected sound paths do not contribute ($F_{\mathrm{P,M,ddec}} = 0$) if the d_{CPA} is less than $2H/\tan\psi_c$.

The contributions of the direct, 1st seabed reflected and multiple reflected sound paths to the propagation factor can then be added:

$$F_{\mathrm{P,ddec,LF}} = F_{\mathrm{P,D,ddec,LF}} + F_{\mathrm{P,B,ddec,LF}} + F_{\mathrm{P,M,ddec,LF}}, \tag{23}$$

$$F_{\mathrm{P,ddec,HF}} = F_{\mathrm{P,D,ddec,HF}} + F_{\mathrm{P,B,ddec,HF}} + F_{\mathrm{P,M,ddec,HF}}. \tag{24}$$

The LF and HF contributions are then merged to obtain a smooth solution for the propagation factor as function of dimensionless wavenumber $k_c d_s$. There are various options for a smooth merging of the LF and HF approximations. For the SSCI method, we have chosen

$$F_{\mathrm{P,ddec}} \approx \left(F_{\mathrm{P,ddec,LF}}^{-2} + F_{\mathrm{P,ddec,HF}}^{-2}\right)^{-1/2}. \tag{25}$$

This choice led to an acceptable agreement with the full solution, as illustrated by the model verification examples in Fig. 3. A reference implementation of the SSCI formulas [see Eqs. (6)–(25)] is provided in a spreadsheet document accompanying this article (see the supplementary material).

C. SSCI simplified

To avoid the complex calculation of the reflection coefficient, a simplified version of the SSCI method (SSCI-sim) is proposed in which the power reflection coefficient is approximated by

$$R_{\mathrm{P}}(\theta_+) \approx \begin{cases} R_{\mathrm{P}}(0) = 1 & \text{for } \theta_+ < \psi_c, \\ R_{\mathrm{P}}\left(\frac{\pi}{2}\right) = \left(\frac{\rho_{\mathrm{b}}c_{\mathrm{b}} - \rho_{\mathrm{w}}c_{\mathrm{w}}}{\rho_{\mathrm{b}}c_{\mathrm{b}} + \rho_{\mathrm{w}}c_{\mathrm{w}}}\right)^2 & \text{for } \theta_+ > \psi_c. \end{cases} \tag{26}$$

The effect of this approximation on the calculated propagation factors (LF and HF) is small except at angles near $\theta_+ = \psi_c$, where it is larger for softer sediments (see the supplementary material).

D. SSCI formula analysis

The relative contribution of seabed reflections to the shallow water propagation factor [see Eqs. (23) and (24)] depends on the measurement location and on the sediment type. The measurement location is expressed in terms of the horizontal distance d_{CPA} and the hydrophone depth d_h relative to the water depth H. The sediment type determines the critical seabed angle ψ_c and the angle dependent power reflection coefficient $R_{\mathrm{P}}(\theta_+)$.

Figure 2 shows the relative contributions of the reflected paths (B and M) to the propagation factor for a "coarse sand" sediment (see Table I for the sediment parameters).

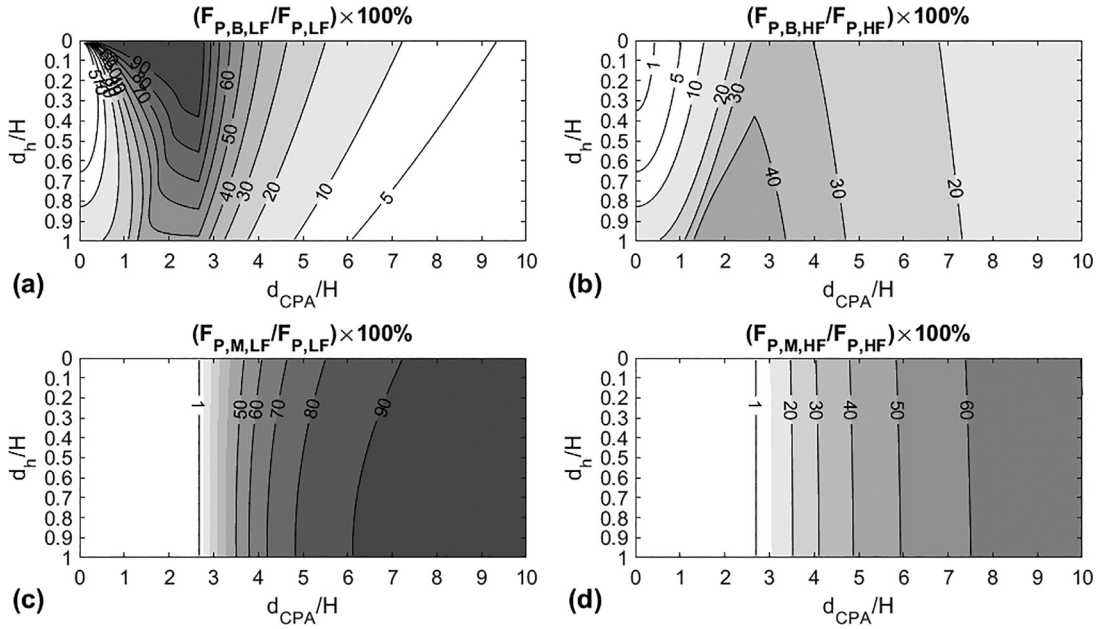

FIG. 2. Relative contributions of the 1st seabed reflection (B, upper graphs) and of multiple subsequent reflections (M, lower graphs) to the low-frequency (left graphs) and high-frequency (right graphs) approximations to the shallow water propagation factor, as function of the measurement location (horizontal distance d_{CPA} and depth d_{h}) relative to the water depth H, for a coarse sand sediment. Darker colors indicate a higher contribution to the propagation factor; the numbers with the contour lines quantify the percentages shown in the header of each graph.

In the low-frequency limit $k_w d_s \ll 1$, the contribution of the 1st seabed reflection (B) is significant [see Fig. 2(a)], particularly in the upper part of the water column at horizontal distances from 1 to 3 times the water depth, because of the relatively low level of the direct path due to the dipole effect. At these distances and in the high-frequency limit $k_w d_s \gg 1$, the contribution of the 1st seabed reflection [see Fig. 2(b)] is the greatest in the lower half of the water columns, although it contributes less than 50% to the total propagation factor.

At horizontal distances greater than 3 times the water depth, the multiply reflected paths (M-paths) dominate the propagation [see Figs. 2(c) and 2(d)]. At shorter horizontal distances, up to 3 times the water depth, contributions of M-paths affect the propagation factor with less than 10%.

PL is lower (propagation factor F_{P} is larger) in shallow water than in deep water due to the contributions of seabed reflections. The difference increases with increasing distance (d_{CPA}). The difference decreases when the sediment is softer than the coarse sand that was assumed for Fig. 2 (see supplementary material).

III. RNL CALCULATION

Two different measures of URN are considered by ISO 17208, namely SL and RNL. Both are in widespread use, and they are sometimes conflated.

It follows from the definition of SL (symbol L_S) that it can be used to evaluate SPL (symbol L_p) via the PL (symbol N_{PL}):

$$L_p = L_S - N_{\mathrm{PL}}. \tag{27}$$

Despite the apparent simplicity of Eq. (27), SL is not related in a simple way to SPL because of the presence of PL.

TABLE I. Numerical test cases used to compare SSCI and SCA methods with more detailed but elaborate propagation loss models. The simplified sediment reflection coefficient is the value at normal incidence [Eq. (12)]. The sound speed and density of seawater are 1490 m/s and 1027 kg/m^3, respectively. The term atan$(2H/d_{\mathrm{CPA}})$ is used in Eq. (12) for the minimum integration angle, θ_{min}.

Parameter / Test case	Test case A	Test case B	Sediment properties: Type	Coarse sand	Fine silt
Water depth H	100 m	50 m	Median grain size	0.5 ϕ	6.5 ϕ
CPA-distance d_{CPA}	80 m	200 m	Sound speed ratio $c_{\mathrm{b}}/c_{\mathrm{w}}$	1.2503	1.0239
d_{CPA}/H	0.8	4	Critical angle (ψ_{c})	37°	12°
atan$(2H/d_{\mathrm{CPA}})$	68°	27°	Density ratio $\rho_{\mathrm{b}}/\rho_{\mathrm{w}}$	2.231	1.513
Hydrophone depth d_{h}	80 m	49 m	Attenuation per wavelength β_{b}	0.87 dB	0.17 dB
Angle θ_{0-}	45°	14°	Reflection coefficient R_{P}, case A	0.28	0.05
Angle θ_{0+}	56°	14°	Reflection coefficient R_{P}, case B	0.93	0.25
Source depth	5 m	5 m	Simplified reflection coefficient R_{P}	0.22	0.05

https://doi.org/10.1121/10.0036140

The benefit of accepting this complexity is that, once PL is known or can be evaluated at some location of interest, one can calculate SPL at that location (e.g., for a sound map).

The SSCI method calculates SL, not RNL. However, for some applications, RNL is needed (e.g., for quiet ship certification). RNL is defined for deep water, and for the measurement conditions specified by ISO 17208-1:2016 (2016), as

$$L_{\mathrm{RN}} = L_p + 10\log_{10}\left(\frac{r^2}{r_0^2}\right)\mathrm{dB}, \tag{28}$$

which implies that

$$L_p = L_{\mathrm{RN}} - 10\log_{10}\left(\frac{r^2}{r_0^2}\right)\mathrm{dB}, \tag{29}$$

where L_p is the SPL at the measurement location, under the specified conditions. Equation (29) is simple to apply because SPL can be estimated (at the specified measurement location in deep water) by subtracting $10\log_{10}(r^2/r_0^2)$dB from RNL.

RNL is not defined in shallow water. It is a measure of the sound that would be radiated if the same ship, under the same operating conditions, was placed in deep water. Section 7.3 of ISO/DIS 17208-3 (2023) proposes converting the SL that is measured in shallow water to a RNL, similar to what would have been measured in deep water, according to ISO 17208-1:2016 (2016). This conversion can be made by subtracting the correction given by the formula proposed in ISO 17208-2:2019 (2019):

$$L_{\mathrm{RN}} = L_{\mathrm{S}} + 10\log_{10}\frac{14(kd)^2 + 2(kd)^4}{14 + 2(kd)^2 + (kd)^4}\,\mathrm{dB}. \tag{30}$$

Results reported in this paper are not represented through the RNL metric. However, they can be derived using Eq. (30) over SLs from Sec. V, available in the supplementary material.

IV. VERIFICATION

Two numerical test cases were selected for comparing the PL calculations from the SCF, SCA, and SSCI methods with results from the OASES wavenumber-integration model (Schmidt, 2004; Schmidt and Jensen, 1985). For range-independent environments, a wavenumber-integration model computes the exact acoustic field and is thus widely used for computing benchmark solutions. One test case represents measurements at a CPA distance that is less than the water depth ("deep water"), and the other is for measurements at a CPA distance of 4 times the water depth ("shallow water"). The results shown in Fig. 3 are for a single hydrophone and for two seabed types: a coarse sand and a fine silt sediment. The sediment properties are taken from Table 4.18 in Ainslie (2010). Table I gives an overview of the parameters for the two test cases.

For the deep water case A, the SCF method agrees well with the coherent OASES model, particularly above 100 Hz. Below 100 Hz, coherent effects of the bottom reflected rays lead to differences. For the shallow water case B, coherent effects lead to somewhat larger differences between SCF and OASES. Here, the OASES calculation results represent the average propagation factor over 11 logarithmically spaced frequencies per decidecade band for case A and 101 frequencies for case B. The other results are calculated at the decidecade band center frequency, where the SCF and SSCI results include an analytical frequency band average.

The SCA and SSCI methods provide a smooth approximation to the PL that does not predict the peaks and valleys at intermediate frequencies (about 200 and 400 Hz for case A and about 600 and 1200 Hz for case B) that are associated with the first reflection at the sea surface. The height of these peaks corresponds with the depth of the nulls in the propagation factor. The peaks are lower for the coarse sand than for the fine silt sediment, because of the stronger contribution from seabed reflections at these frequencies. Predicting the frequency of these sharp peaks requires precise input values for geometry and sediment parameters that are often lacking. Consequently, the presence of such peaks in the calculated PL can lead to overestimation of the SL in the corresponding frequency bands [see Ainslie *et al.* (2024a)].

The simplified reflection loss calculation [SSCI-sim, Eq. (26)] results in an ∼1 dB higher PL for case A and an ∼2 dB higher PL for case B with a fine silt sediment.

These results confirm that the SSCI method agrees better with the OASES and SCF predictions at frequencies above about 1 kHz, compared with the SCA method, which underestimates PL by 1–2 dB. Therefore, the SSCI is proposed as a more accurate formula for calculating PL that remains straightforward to implement and robust to uncertainties in the input parameters.

V. VALIDATION WITH SATURN DATA

A. Experimental design

URN tests executed in the scope of the SATURN project allowed the measurement of a varied set of testing procedures and also included the draft version of the shallow water standard, ISO/DIS 17208-3 (2023). Including also the deep water standard procedure (ISO 17208-1:2016, 2016) in the test campaign made it possible to obtain reference underwater sound levels produced by the vessel under specific operating conditions, permitting the evaluation of the accuracy of the shallow water results obtained using the draft procedure.

One of the major advantages of the shallow water standard is its flexibility, especially in terms of test site selection, execution, and instrumentation deployments. It comprises multi-hydrophone deployments, such as vertical and horizontal three-hydrophone line arrays, and single-hydrophone ones, whether using surface buoy, bottom-mounted or bottom-tethered strategies. The selection of one

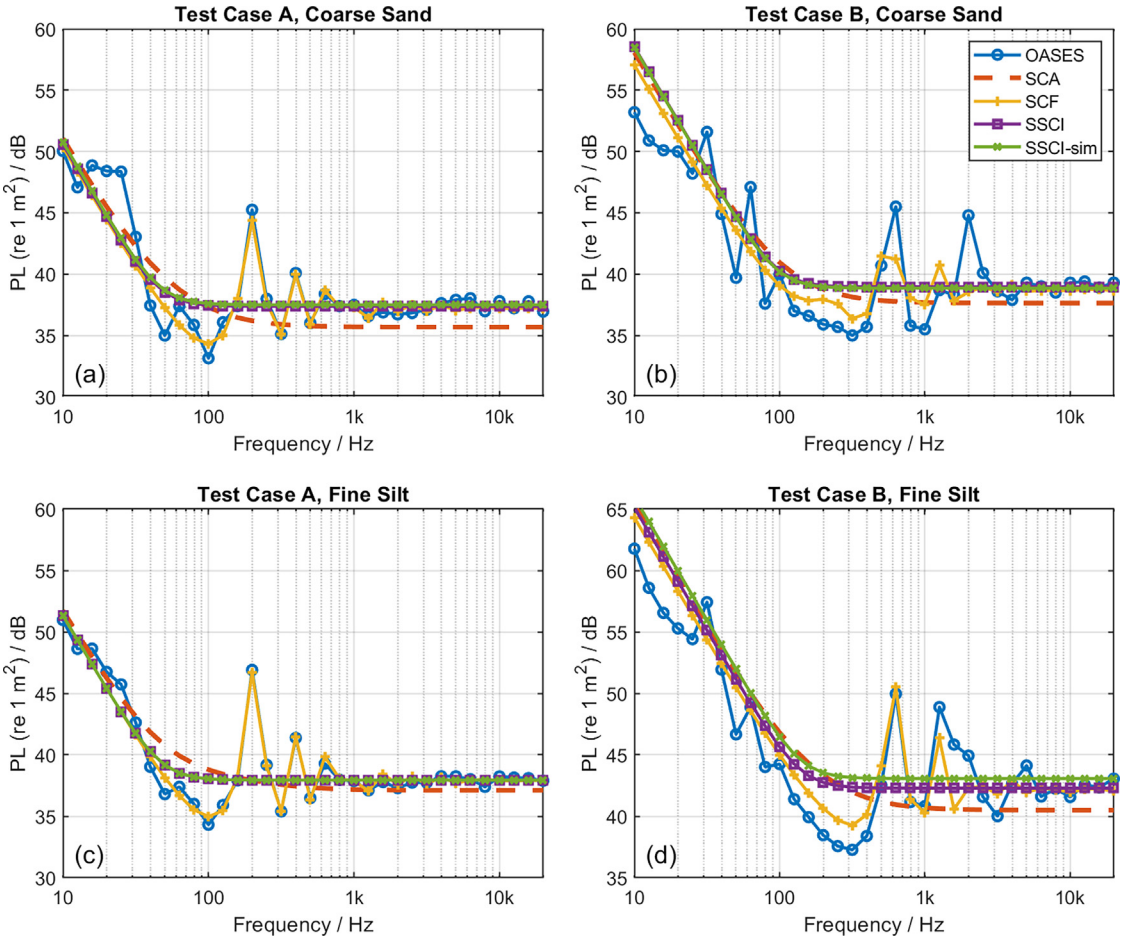

FIG. 3. Calculated propagation loss versus frequency for (a) test case A with a coarse sand sediment, (b) test case B with a coarse sand sediment, (c) test case A with a fine silt sediment, and (d) test case B with a fine silt sediment, comparing results from the wavenumber integration model (OASES) with the various approximations (SCA, SCF, and SSCI).

or three hydrophones is open to the user's choice, but not the specifics of each deployment, which are restricted by the relation of the site depth and CPA distance. For CPA distances less than the site depth ($d_{\mathrm{CPA}} < H$), two deployment configurations are allowed: (i) a vertical line array (VLA) compliant with the deep water requirements (observation angles of the hydrophones of 15°, 30°, and 45°) or (ii) a single-hydrophone deployment (SHD) with an observation angle within [15°, 45°]. For CPA distances greater than the site depth ($d_{\mathrm{CPA}} > \mathrm{H}$), three configurations are possible: (i) a VLA with the shallowest hydrophone at least 15 m from the surface and a distance between hydrophones of 10 m or above, (ii) a SHD placed in the lower half of the water column, or (iii) a horizontal line array (HLA) within the allowed CPA range ($[H, 5 \cdot H]$).

The SATURN tests included five different equipment deployments for the shallow water measurements, represented in Fig. 4 and identified as (A) to (E). The executed

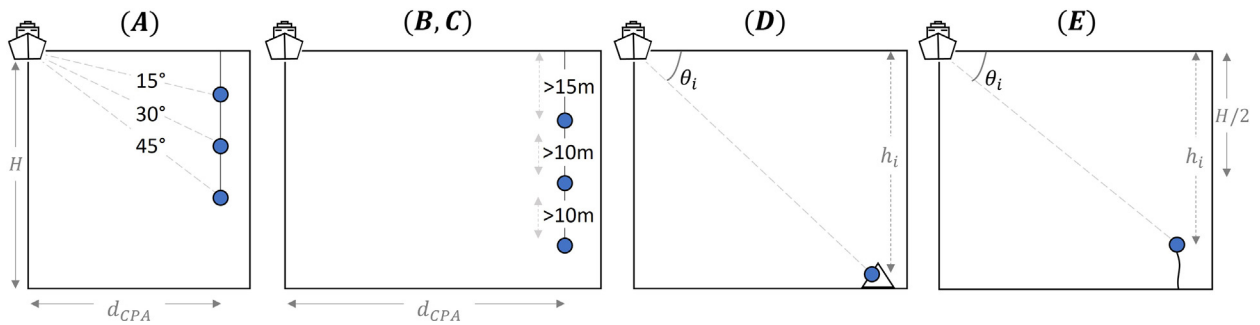

FIG. 4. Drawings of ISO/DIS 17208-3 (2023) deployments tested during the SATURN measurements [(A)–(E)]. Solid circles represent deployed hydrophones. The restrictions for each deployment strategy are provided in Table II ("Deployment restrictions" column). d_{CPA} stands for CPA distance, H for site depth, h_i for hydrophone depth, and θ_i for observation angle.

https://doi.org/10.1121/10.0036140

testing matrix comprised measurements carried out using VLAs whether at CPA distances less than the site depth [deployment (A)] or greater than it [deployments (B) and (C)], also performing recordings based on SHDs as bottom-mounted [deployment (D)] and bottom-tethered [deployment (E)]. HLAs were not directly tested, although it was possible to emulate them using single-hydrophone recordings at different CPA distances, further explained later. On the other hand, from the VLAs it was possible to derive SHDs, when the restrictions of the draft standard were met.

Shallow water measurements included in this study cover three different site depths (40, 50, and 80 m), four target CPA distances (50, 100, 150, and 200 m), three processing geometries (VLA, HLA, and SHD), and five different deployments [(A) to (E); previously shown in Fig. 4]. On the other hand, the deep water measurements, performed under the deep water standard, were executed on two different days, covering a site depth of approximately 200 m and a target CPA of 100 m, using three-hydrophone VLAs to deploy the equipment. These measurements were recorded on seven out of the nine days of the SATURN test campaign and are summarized in Table II.

B. Equipment

The equipment was deployed daily as VLA or SHD. The VLA used a surface buoy to continuously monitor its position and synchronize the hydrophones' time [by Global Positioning System (GPS) time and pulse per second (PPS) protocol]. The surface buoy was usually kept in a stable position using an auxiliary mooring line. It was also deployed as a drifting buoy for a limited space of time during one of the testing days. SHDs were bottom-mounted and bottom-anchored and were manually synchronized with a support laptop before putting the hydrophones into water, having a time lag of 1 s at the most. The hydrophones used were model icListen HF RB9 from Ocean Sonics (Truro Heights, Canada) (nominal sensitivity re 1 V/μPa of –177 dB), configured to acquire data continuously at a sampling rate of 128 kHz. Their proper functioning was checked daily at the start and end of the day using a pistonphone (model 42AC; G.R.A.S., Twinsburg, OH). The communication buoy used to provide time synchronization for the hydrophones was a model BOSS W drifting buoy from Ocean Sonics.

Two GPS receivers were used to monitor the drifting buoy and vessel position (models A631 and VS1000; Hemisphere, Scottsdale, AZ). They gathered data at a sampling rate of 1 Hz, providing positions with an accuracy of ~0.25 m.

The sound speed of the water column was recorded by a conductivity, temperature, and depth (CTD) transducer at a sampling rate of 1 Hz (model Concerto 3; RBR, Ottawa, Canada). It was placed close to the deepest hydrophone in the VLAs, recording the site sound speed, which varied from 1523 m/s to 1534 m/s during the trials. The CTD was also used to gather the depth of the deepest hydrophone and compute the approximate hydrophone cable drift angle. These angles were generally greater than desired [ISO 17208-1:2016 (2016) recommends it to be less than 5°], while the worst cases happened in deep water, likely caused by stronger water currents. This influence was evaluated, concluding it had a negligible impact in deep water measurements and even lower impact in shallow water.

During the tests, internal software was used to continuously compute the vessel-buoy distance, providing the required course to meet the target CPA for each pass, notably reducing the number of invalid passes and decreasing the testing time and fuel consumption. Another internal software was used to log execution information for each testing day. Some of these data were relative to the deployment information (e.g., site depth, hydrophone depths and positions, installing position for the GPS on the vessel, etc.). This logbook also contained information about the test execution, gathering data for each record as the vessel side, target CPA, target vessel speed, operating conditions (e.g., engine power, engine rpm), initial and end time of the run, etc. This logbook was used later during the data processing, employing most of its information to automate and optimize the task.

C. Data processing

1. Data quality verification

Data quality verification is crucial in reporting vessels' underwater sound signatures. Measuring procedures remark on the importance of verifying the measuring chain daily

TABLE II. Summary of URN measurement from the SATURN test campaign used in this study.

Deployment IDs	Testing procedures	Testing dates[a]	Measuring geometries	Site depths (m)	Target CPAs (m)	Deployment restrictions	Hydrophone deployments
	ISO 17208-1:2016 (2016)	2 Nov and 8 Nov	VLA	200	100		15°, 30°, 45°
(A)	ISO/DIS 17208-3 (2023)	5 Nov	VLA	80	50	$d_{CPA} < H$	15°, 30°, 45°
(B)	ISO/DIS 17208-3 (2023)	6 Nov	VLA	50	>50	$d_{CPA} > H$	>15 m[b]
(C)	ISO/DIS 17208-3 (2023)	7 Nov	VLA	80	100, 150, 200	$d_{CPA} > H$	>15 m[b]
(D)	ISO/DIS 17208-3 (2023)	9 Nov	SHD	40	100	$h_i > H/2$	Bottom-mounted
(E)	ISO/DIS 17208-3 (2023)	10 Nov	SHD	40	100	$h_i > H/2$	Bottom-tethered

[a]The SATURN test campaign in Las Palmas took place in November (Nov) 2022.
[b]Distance from the surface.

and define constraints regarding the distance accuracy measurement, vessel speed, and others. The objective regarding the data quality verification during this study was to perform the checks required by the standard and to go a step further to ensure the greatest reachable data quality used to get the results.

For on-site verifications, the primary check was to confirm the proper functioning of the hydrophones twice per day, using a pistonphone before the deployment and after the recovery, which produces a pure tone in air with a SPL (re 20 μPa) of 134 dB at 250 Hz. Levels recorded by the hydrophones during the SATURN test campaign were within ± 0.15 dB from the expected value, confirming their proper functioning during the trials.

Additional verifications performed over the testing conditions were also performed to check (i) buoy drift, (ii) vessel course, (iii) CPA distance, and (iv) vessel speed over the ground. These analyses helped determine the quality of the measuring conditions for each recording and supported the choice of valid runs used later in the computation of the final vessel signatures. Part of this information was also employed to summarize the tested conditions per day, using the measured CPA and the average vessel speed of the processing window (example shown in Fig. 5).

The verifications described so far were focused on instrumentation checks and executed testing conditions. Additional verifications performed over acquired sound signals were also included in the data quality verification process. In that case, a visual inspection of individual SPLs recorded by the hydrophones, represented in 1 Hz resolution narrowband spectra, was carried out (examples provided in Figs. 6 and 7). Although this is not an activity required by the standards, it is a good practice that was tremendously helpful in understanding acquired sound data and detecting some unexpected behaviors of the test site and vessel under test. The selected test site had strong currents, causing flow noise in most measurements up to frequencies around 100 Hz; such parasitic noise was identified in this step (see Fig. 6). Additionally, abnormal vessel behavior was detected at speeds below ~10 kn (~5.1 m/s), where high amplitude tones appeared (see Fig. 7). Their features were unstable, so the selected testing speed to perform the analyses of this paper is focused on the target speed over the ground of 11 kn (5.7 m/s), which was confirmed to have a consistent performance.

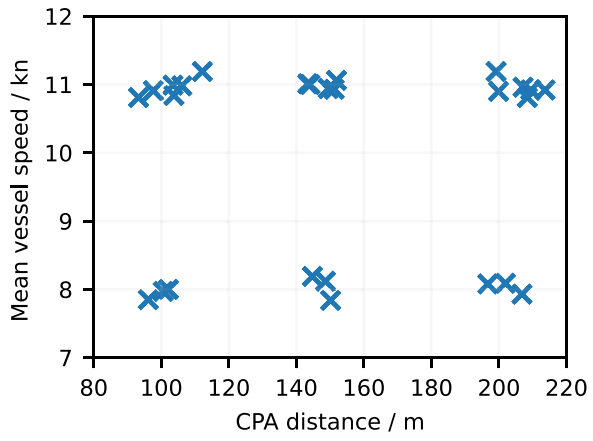

FIG. 5. Summary of valid runs for one day of the SATURN test campaign (7 November). Measurements performed at target vessel speeds (over ground) of 8 and 11 kn (4.1 and 5.7 m/s) and three CPAs (100, 150, and 200 m).

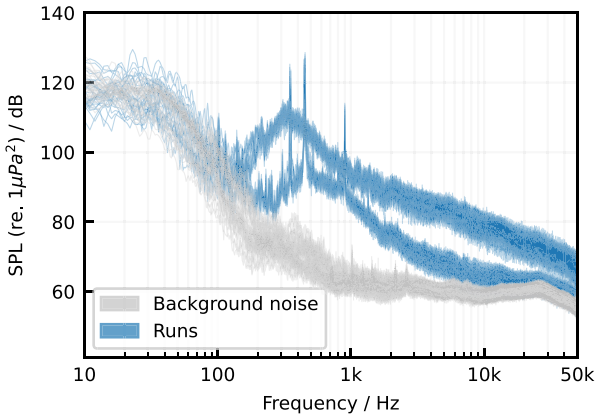

FIG. 6. Measured SPL (re 1 μPa^2) in 1 Hz bands for background noise and vessel transits at 8 and 11 kn (4.1 and 5.7 m/s) for one testing day (6 November). Background noise measurements were recorded daily after deploying the equipment and before its retrieval, meeting ISO 17208-1:2016 (2016) requirements.

Only data passing these requirements were considered suitable for the following step of the processing workflow and, therefore, used to obtain the vessel signatures.

2. Post-processing

The deep water results were processed according to the ISO 17208-1:2016 (2016) standard, obtaining the relevant RNLs, later converted to SLs as described in ISO 17208-2:2019 (2019) [Eqs. (31) and (32)]:

$$L_{S,\mathrm{ISO}} = L_{\mathrm{RN}} + \Delta L_{\mathrm{ISO}}, \tag{31}$$

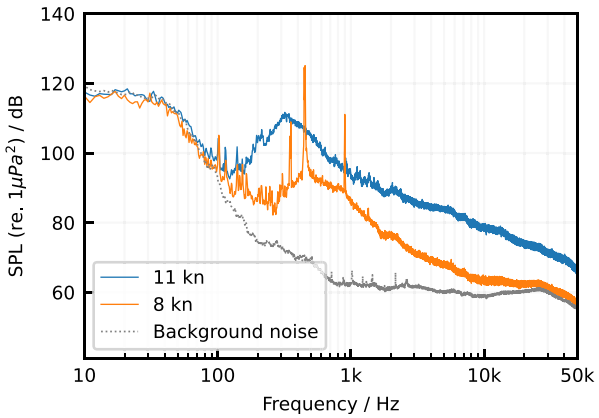

FIG. 7. Median SPL (re 1 μPa^2) in 1 Hz bands for background noise and vessel transits at 8 and 11 kn (4.1 and 5.7 m/s) derived from Fig. 6 data (considering 6 runs for 11 kn, 5 runs for 8 kn, and 13 recordings for background noise, with each run or recording composed of three spectra, one per hydrophone).

https://doi.org/10.1121/10.0036140

TABLE III. Processing parameters used to get SLs. ISO/DIS 17208-3 (2023) measurements [deployment IDs (A) through (E)] were processed under the SCA, SSCI, and SSCI-sim methods. Parameters in italics indicate those that were not measured but derived from available resources [see Table IV.18 in Ainslie (2010)]). The assumed seabed type was fine sand, based on information of the test site from EMODnet (2024). M, number of runs processed; H, site depth; h_i, hydrophone depth; d_s, nominal source depth; c_w, sound speed in water; c_b, sound speed in seabed; ρ_w, mass density in water; ρ_w, mass density in seabed; β_b, attenuation per wavelength in seabed.

Deployment IDs	M	H (m)	CPA ranges (m)[a]	h_i (m)	d_s (m)	c_w (m/s)	c_b (m/s)	ρ_w (kg/m^3)	ρ_b (kg/m^3)	β_b (dB)
ISO 17208-1:2016 (2016)	20	200	91–112	27, 58, 100	3.9	1527	N.A.	N.A.	N.A.	N.A.
(A)	4	80	42–61	13, 29, 50	3.9	1530	*1750*	*1000*	*1900*	*0.925*
(B)	4	50	50–61	20, 27.5, 35	3.9	1534	*1750*	*1000*	*1900*	*0.925*
(C)	12	80	79–106, 143–152, 199–208	35, 55, 75	3.9	1531	*1750*	*1000*	*1900*	*0.925*
(D)	4	40	99–102	39.8	3.9	1530	*1750*	*1000*	*1900*	*0.925*
(E)	8	40	85–102	38	3.9	1530	*1750*	*1000*	*1900*	*0.925*

[a]Specific CPA values per run are provided within the supplementary material.

$$\Delta L_{\mathrm{ISO}} = -10\log_{10}\frac{14(kd)^2 + 2(kd)^4}{14 + 2(kd)^2 + (kd)^4}\ \mathrm{dB}. \tag{32}$$

The deep water results are used as the reference SL. The parameters used for the computation are provided in the first row of Table III. As for the shallow water results, their processing was compliant with ISO/DIS 17208-3 (2023), which directly returns results as SLs. This section focuses on the processing of the shallow water measurements.

ISO/DIS 17208-3 (2023) relies on the post-processing of ISO 17208-1:2016 (2016), so most of its steps are identical. Only the background noise correction and the distance adjustment differ, which is explained later.

The process starts by identifying the time instant where CPA is reached, to later cut the recorded time signal for a processing window covering a range of $\pm 30°$ from the CPA position. The corresponding time interval is processed to obtain the decidecade SPL spectrum. This step is not detailed in ISO 17208 standards, so for the SATURN project data, the spectral processing was carried out using the fast Fourier transform over 1 s slices, employing a Hann window with 50% overlap. Resulting spectra were then energy-averaged, obtaining a narrowband spectrum of 1 Hz resolution. This spectrum was visually inspected to confirm data quality and represented using wider frequency bands, returning the SPL spectra in decidecade bands.

SPL spectra were employed to resume the steps described in ISO/DIS 17208-3 (2023) according to the following procedure. First, the background noise correction is applied over all those bands where the signal-plus-noise-to-noise level difference is above 3 dB (the first of the mentioned differences against the deep water procedure, which does not apply it above 10 dB). Second, the spectral sensitivity adjustments are performed according to each hydrophone spectral response, obtaining what the standards refer to as the sensitivity-adjusted sound pressure level (L_p). Then, PL is computed using the SCA method, as described in the draft of the shallow water standard, obtaining the corresponding SL per hydrophone and run. Additionally, for the purpose of this study, PL was also computed using the SSCI and SSCI-sim methods, obtaining the corresponding SL per hydrophone and run for these two additional approaches. The parameter values used to process each set of data are gathered in Table III.

Results obtained in the previous step correspond to a certain hydrophone and run and are to be averaged to get the final SL for a certain condition. The average SL for each run, $L_S(m)$, is computed as

$$L_S(m) = 10\mathrm{lg}\left[\frac{10^{L_S(m,h_1)/(10\mathrm{dB})} + \cdots + 10^{L_S(m,h_3)/(10\mathrm{dB})}}{N}\right]\mathrm{dB}, \tag{33}$$

where $L_S(m, h_n)$ is the SL for the nth single hydrophone for run m and N is the number of hydrophones. Then, the final condition SL, L_S, is obtained averaging the SL of four runs as:

$$L_S = \frac{\sum_{m=1}^{m=M} L_S(m)}{M}, \tag{34}$$

where M is the number of runs.

Each of the methods explained to obtain SLs requires a set of input parameters, which vary between procedures. Table IV indicates the required parameters per computation method (also including those for the deep water standard), summarizing inputs needed per procedure and indicating which of those values are measured (solid dots) or have to be obtained from alternative resources (x symbols).

Results obtained before applying the PL correction (sensitivity-adjusted sound pressure level; L_P) are provided

TABLE IV. Parameters required to compute the PL for the described methods. The solid dots denote the parameters measured during the test campaign, the x symbols those that were estimated. H, site depth; d_{CPA}, CPA distance; h_i, hydrophone depth; d_s, nominal source depth; c_w, sound speed in water; c_b, sound speed in seabed; ρ_w, mass density in water; ρ_b, mass density in seabed; β_b, attenuation per wavelength in seabed.

PL method	H	d_{CPA}	h_i	d_s	c_w	c_b	ρ_w	ρ_b	β_b
ISO17208-2	•	•	•	•	•				
SCA	•	•	•	•	•	x			
SSCI	•	•	•	•	•	x	x	x	x
SSCI-sim	•	•	•	•	•	x	x	x	

as additional material to this article, allowing reproduction of the results of the paper whether using the described PL methods (SCA, SSCI, SSCI-sim) or any other method.

D. Measurement summary

Measurements were carried out in Las Palmas (Canary Islands, Spain) in November 2022 for 11 consecutive days, while 9 of them were used to execute the recordings. Measurements compliant with the ISO 17208-1:2016 (2016) and ISO/DIS 17208-3 (2023) procedures were executed on two and five different days, respectively (previously shown in Table II). The vessel characterized during the test campaign was the *Ángeles Alvariño* research vessel, belonging to the Spanish National Institute of Oceanography (referred to as IEO for its Spanish name, *Instituto Español de Oceanografía*). Its main vessel particulars are vessel length of 47 m, ship beam of 10.5 m, ship draft of 5.6 m, maximum speed of 13 kn (6.7 m/s), diesel-electric propulsion (nominal power of 900 kW), and a fixed pitch propeller with five blades (diameter of 2.9 m).

The equipment setup (hydrophones, GPSs, and CTD) was deployed and recovered daily during the test campaign, spending more than 45 h in water. Almost 190 vessel passes gathering different operating conditions of the vessel were recorded, with another 80 background noise measurements. Tests results from this paper focus on a target speed—over the ground—of 11 kn (5.7 m/s).

Measurements carried out in shallow waters were regrouped according to their processing geometry (VLA, SHD, and HLA), obtaining individual SLs as the combination of measurements carried out under the same conditions within a time slot not exceeding 4 h. Combining acquired data carefully allowed for an increase in the number of available results foreseen, deriving SHDs from VLAs, or emulating HLAs based on SHDs tested at different CPA distances. Thus, the numbers of condition SLs obtained were 6 for VLAs, 3 for HLAs, and 15 for SHDs.

Table V gathers some details of the data used to get the condition SLs per processing geometry. Obtained SLs summarized in Table V were processed as described in Sec. V C 2, reporting those from shallow waters under different methods (SCA, SSCI, SSCI-sim), and are used to compare the methods' results later in Sec. V F.

HLA results were obtained using measurements from a single hydrophone [data from deployment (C)] varying the CPA distance. According to the standard's requirements, the HLAs use 3 hydrophones and require 4 runs per condition, so each result combines 12 spectra. For the HLAs analyzed, the number of samples required was maintained by testing at 3 CPA distances and 4 runs per distance, thus obtaining the expected 12 spectra. The mentioned strategy complies with the standard except in minor details. SHDs were fully compliant with the standard requirement, where the number of runs is kept at four, requiring only 4 spectra per result. For both HLAs and SHDs, the SLs per condition were obtained by applying a linear averaging over all the corresponding samples, as required by the standard for measurements of different passes [Eq. (34)].

The analysis bandwidth includes the decidecade bands from 125 Hz to 20 kHz. The lower limit is set due to the flow noise issue experienced and explained in the data quality section (Sec. V C 1), while the ISO/DIS 17208-3 (2023) recommendation sets the upper limit. The reason for doing so [instead of reporting up to 50 kHz as ISO 17208-1:2016 (2016) suggests] is that at frequencies above 20 kHz, the sound absorption of water has an impact that increases with the distance. ISO/DIS 17208-3 (2023) allows a great variety of CPA distances, so the PL computation may include the water absorption. That correction is not included in the standard, and the suggested upper frequency is limited to 20 kHz. Section VII A includes an approach that accounts for water absorption and may improve the accuracy of the results if reporting them above 20 kHz.

E. Reference SLs

ISO 17208-1:2016 (2016) was tested on two different days using a three-hydrophone VLA to record the vessel's underwater sound in deep water. The procedure was measured several times at a speed over the ground of around 11 kn, also performing vessel passes at different angles against the current. Measurements were processed to get five condition RNLs and then derive the corresponding SLs (Fig. 8) according to ISO 17208-2:2019 (2019) (parameters used available in Table III).

The consistency of obtained results was explored by computing the dispersion of the obtained vessel signatures, returning a standard deviation of ∼1 dB within the 100 Hz to 20 kHz frequency range (Fig. 9). The demonstrated consistency of the results supported using the deep water results to rate results obtained under the draft ISO/DIS 17208-3 (2023) standard. The mean deep water SL was computed

TABLE V. Summary of results obtained per processing geometry to be used to compare the methods. $VLA_{ISO\text{-}1}$ results are compliant with the ISO 17208-1:2016 (2016) description, while the others meet ISO/DIS 17208-3 (2023) requirements.

Processing geometries	Used deployments	Site depths (m)	Target CPAs (m)	Hydrophone depths (m)	Used spectra	Obtained SLs
$VLA_{ISO\text{-}1}$	ISO 17208-1:2016 (2016)	200	100	27–100	60	5
VLA	(A), (B), (C)	50, 80	50, 100, 150, 200	13–75	60	6
HLA	(C)	80	100, 150, 200	35–75	36	3
SHD	(A), (B), (C), (D), (E)	40, 50, 80	50, 100, 150, 200	13–75[a]	60	15

[a]This depth range includes one bottom-mounted hydrophone and one bottom-tethered hydrophone (at 20 cm and 2 m from the seabed).

https://doi.org/10.1121/10.0036140

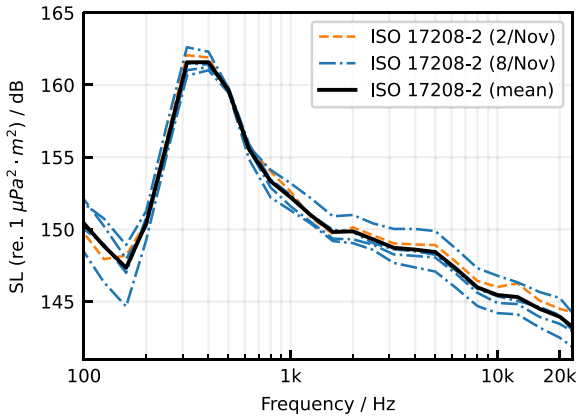

FIG. 8. Vessel's SL in decidecade bands from two different days measured according to ISO 17208-1:2016 (2016) at 11 kn [reported as SL in compliance with ISO 17208-2:2019 (2019)]. The mean SL is represented with the solid line.

(solid line from Fig. 8) and used later as the reference curve to compare with shallow water results.

F. Method comparison

Different SLs were obtained for deep and shallow water to characterize the underwater sound produced by a certain vessel, as summarized in Table V. SLs measured on two days in deep water were averaged as described in Sec. V E and used as the reference to rate the accuracy of shallow water results.

Shallow water recordings characterized the same vessel under equal operating conditions as the deep water measurements and were processed under three different PL approaches (SCA, SSCI, and SSCI-sim). The deep water reference values come from VLA deployments, while those from shallow water cover the three accepted strategies described in ISO/DIS 17208-3 (2023): VLA, HLA, and SHD (for VLA, HLA, and SHD results, see Table V).

Figure 10 compares shallow water results against the deep water reference: Each column of the panel corresponds to a certain deployment strategy, while each row has a different PL method used to derive the shallow water results. A vertical comparison of subplots allows the accuracy reached by the SCA and the enhanced PL methods (SSCI and SSCI-sim) against the deep water reference (thick dashed line) to be explored. Furthermore, the horizontal comparison shows the accuracy and scattering of the results obtained under the explored deployments (VLA, HLA, and SHD) for each PL method.

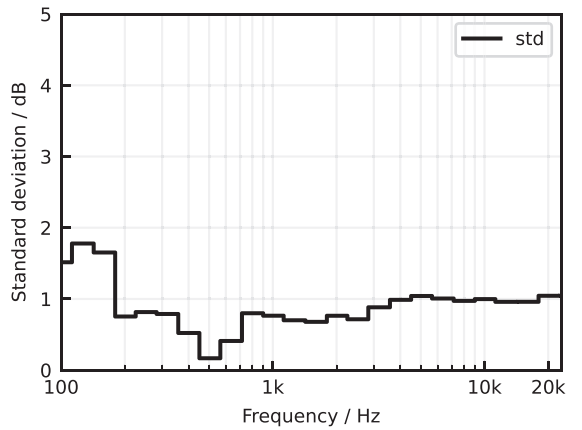

FIG. 9. Decidecade standard deviation from SL measurements performed at 11 kn and reported in Fig. 8.

The difference of the results, obtained as the mean of the SL difference of each subplot curve from Fig. 10 against the deep water reference, is provided in Fig. 11. This figure confirms that both enhanced methods improve the original accuracy reached by the SCA method (∼2 dB improvement for most of the decidecades within the reported bandwidth).

The unbiased standard deviation of reported shallow water SLs from Fig. 10 is shown in Fig. 12, grouping them by deployment geometry, as done in the previous figures. Such a comparison shows a more significant scattering from SHDs, regardless of the PL method used to get the results. The increased scattering in SHDs results is likely produced by the reduced number of samples required to derive each condition SL (VLAs and HLAs require 12 spectra per condition, while SHDs only need 4) and for the variety in terms of hydrophone positions, measuring days, and deployment strategies (bottom-mounted, bottom-tethered, or deployed from a surface buoy). Also, performing measurements at an equal CPA distance for each condition does not allow accounting for different grazing angles between the vessel and the hydrophone, which is a known strategy to increase consistency of results (as done for VLAs and HLAs).

On the other hand, none of the explored PL methods makes a remarkable difference in result scattering, while the one with the lowest average standard deviation is the SSCI (see values from Table VI, last column).

Section VI spans the frequency evaluation of the SSCI method, allowing further study of its performance at those frequencies affected by flow noise in the SATURN data (below 100 Hz).

VI. VALIDATION WITH MMP2 DATA

Additional validation of the SSCI method was carried out by reanalyzing URN measurements from the MMP2 experiment (MacGillivray *et al.*, 2023). The purpose of the MMP2 experiment was to test whether it was possible to obtain reproducible vessel SL estimates in shallow water comparable to ISO-compliant measurements in deep water. This experiment involved repeated URN measurements for three cooperating vessels, using five fixed hydrophone arrays at three test sites (shallow, intermediate, and deep), over a period of three months. SL measurements at the shallow and intermediate test sites were compared to reference measurements obtained at the deep test site. For the present work, SL data from the MMP2 experiment were reanalyzed using the SSCI method for two different array geometries: a VLA deployed at an intermediate depth site and a HLA deployed at a shallow site.

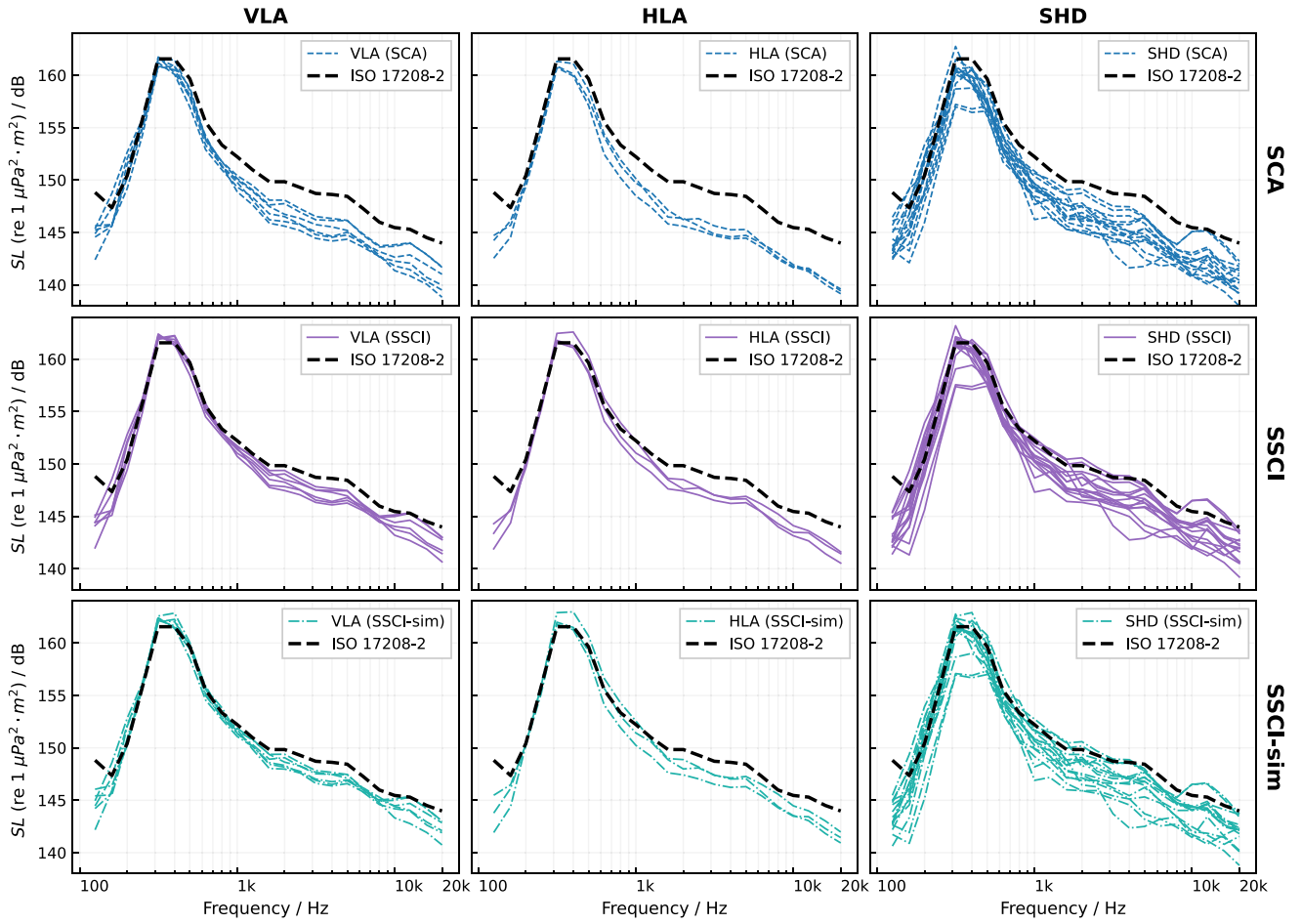

FIG. 10. SCA, SSCI, and SSCI-sim results for SL in decidecade bands in three different deployments (VLA, HLA, and SHD) compared with the deep water reference curve [mean SL from ISO 17208-2:2019 (2019) measurements]. Provided SLs correspond to equal operating conditions measured at 11 kn over the ground, whether from deep water (thicker dashed line) or shallow water (the rest of the curves).

Average SLs for a 167-m-long vessel were computed from an ensemble of ten passes on each array for a narrow range of transit speeds (± 0.25 m/s) and CPA distances (± 20 m) to ensure repeatable conditions. Both single-channel and array-averaged SLs were computed from the array measurements. The bottom loss at the MMP2 test sites was characterized by a stratified seabed with a frequency-dependent critical angle $[\psi_c(f)]$. This was implemented in the SSCI method by using an effective sound speed in the bottom that varied with frequency

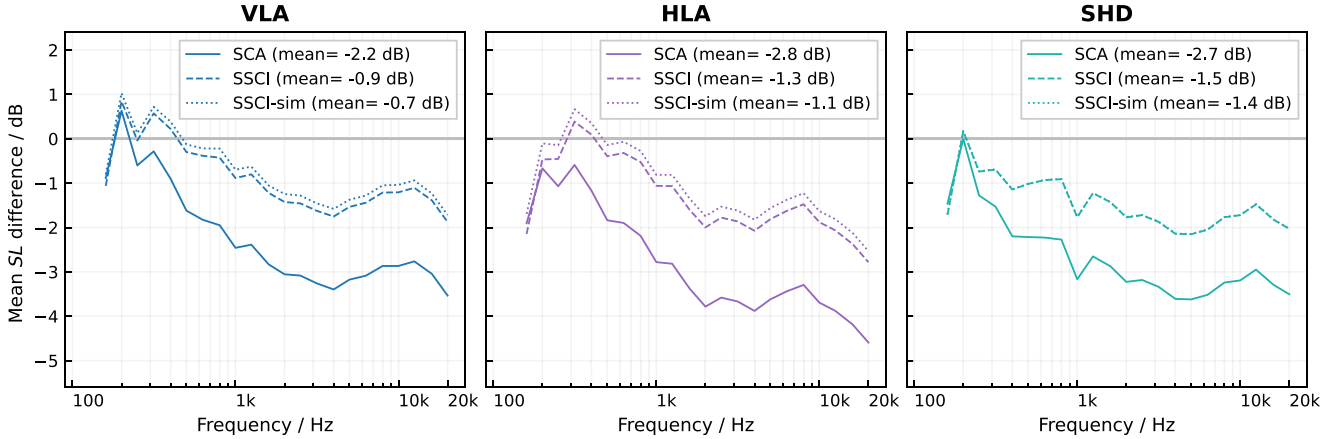

FIG. 11. Mean SL difference against the deep water reference [ISO 17208-2:2019 (2019) curve from Fig. 10] for SCA, SSCI, and SSCI-sim results for VLA, HLA, and SHD geometries. Results for the SHD geometry for SSCI and SSCI-sim are almost identical (curves apparently overlapping in the right subplot).

https://doi.org/10.1121/10.0036140

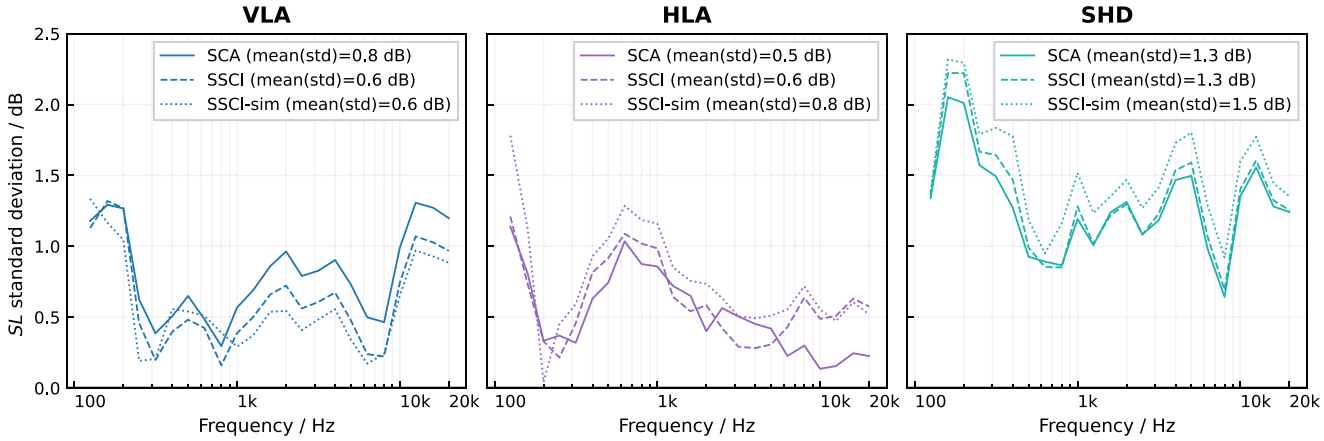

FIG. 12. SL standard deviation for SCA, SSCI, and SSCI-sim results for the explored deployments (VLA, HLA, and SHD). Mean values of shown curves within the reporting bandwidth are provided in the subplot legends and are used to build Table VI.

$$c_b(f) = \frac{c_w}{\cos\psi_c(f)}. \tag{35}$$

Comparison of measurements from the intermediate VLA and shallow HLA with deep water reference SLs (Fig. 13) showed that the SSCI method improved upon the SCA method, particularly at frequencies above 200 Hz.

VII. OTHER FACTORS

A. Water absorption

The draft text of ISO/DIS 17208-3 (2023) enables a wide range of CPA distances to perform the measurements. All analysis to this point has assumed zero or negligible absorption of sound in seawater. For frequencies above 20 kHz, the water absorption can have a significant impact when underwater levels are measured far from the vessel under test (e.g., above 200 m), producing underestimations of several decibels. The maximum allowed CPA of the current shallow water standard draft is 5 times the site depth ($5{\cdot}H$), so the impact of the water absorption can vary drastically.

Hannay *et al.* (2023) proposed to include the water absorption in the SL calculation through an update in the PL term (N_{PL}),

$$N_{PL} = 10\log_{10}\frac{\left(F_P \times 10^{-(a\cdot s)/(10\,\mathrm{dB})}\right)^{-1}}{r_0^2}\,\mathrm{dB}, \tag{36}$$

TABLE VI. Mean standard deviation (in dB) for each PL method and deployment. The method and deployment average (avg.) are provided in the last column and row, respectively (bold values). The data used are extracted from the Fig. 12 legend.

	Mean standard deviation (dB)			
Method and avg.	VLA	HLA	SHD	Method avg. (dB)
SCA	0.8	0.5	1.3	**0.9**
SSCI	0.6	0.6	1.3	**0.8**
SSCI-sim	0.6	0.8	1.5	**1.0**
Deployment avg.	**0.7**	**0.6**	**1.4**	

where F_P is the propagation factor with no absorption, r_0 is the reference distance (1 m), s is the slant range ($s^2 = d_{CPA}^2 + d_i^2$), and α is the water absorption coefficient, which can be estimated as a function of the frequency in kHz (f) using Eq. (2.2) from Ainslie (2010),

$$\alpha = 0.0485 \times \frac{f^2}{76.5^2 + f^2}\ \mathrm{dB/m}. \tag{37}$$

Alternatively, the absorption coefficient can be directly included in the SL computation as an additional term:

$$L_S = L_p + 10\log_{10}\frac{(F_P)^{-1}}{r_0^2}\,\mathrm{dB} + \alpha s. \tag{38}$$

For the SATURN tests, the site depth of the shallow water measurements varied from 40 m to 80 m, with the maximum allowed CPAs of 200 and 400 m, respectively. Figure 14 represents the absorption coefficient in dB [third term from Eq. (38)] for different CPAs of the 80 m depth scenario (H, $2.5{\cdot}H$, $5{\cdot}H$), demonstrating that neglecting the water absorption could underestimate SL in a valid ISO/DIS 17208-3 (2023) scenario up to 6 dB, if considering spanning the reporting bandwidth to 50 kHz (as done in the deep water standard).

The decision made in the draft of the shallow water standard is to limit the reporting bandwidth up to 20 kHz. Possible alternatives that allow spanning the reporting bandwidth (e.g., up to 50 kHz) are to limit the maximum CPA distance further or to include the water absorption correction in the SL computation [as shown in Eq. (38)].

VIII. CONCLUSIONS

The draft shallow water standard (ISO/DIS 17208-3, 2023) tested in the SATURN project specified the SCA method for calculating PL and reporting measured underwater sound as SLs. The test results from the project generally showed good agreement. However, there was an underestimation of SL from mid-frequencies (>500 Hz) by

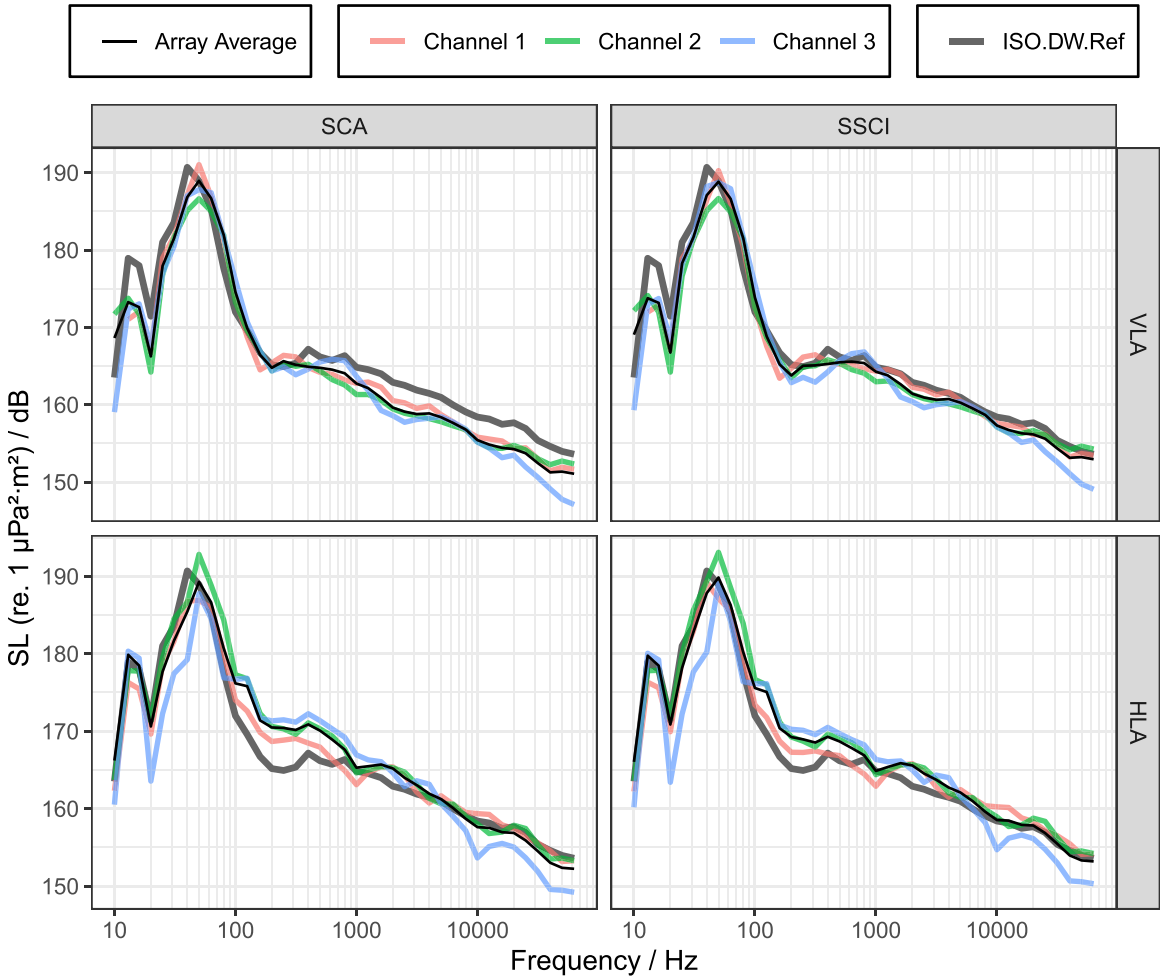

FIG. 13. Single-channel (colored lines) and array-averaged shallow water source levels (thin black line), compared to reference source levels measured in deep water using the ISO 17208-2:2019 (2019) formula (thick gray line), as measured during the MMP2 experiment. (Top) Vertical line array in 66 m water depth at 150 m CPA. (Bottom) Horizontal line array in 31 m water depth at 170 m CPA. (Left) Source levels calculated using the SCA method. (Right) Source levels calculated using the SSCI method.

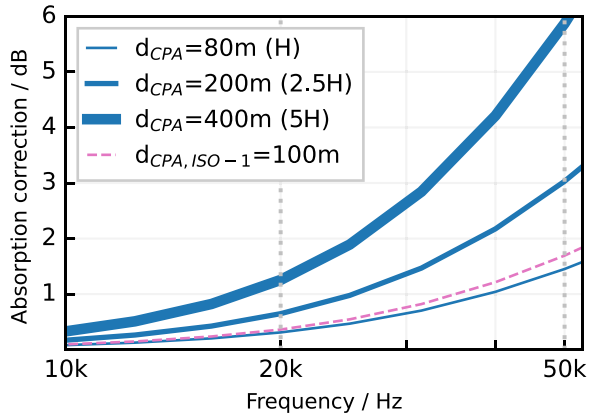

FIG. 14. Water absorption correction for possible scenarios from the SATURN project test campaign. Solid lines represent the water absorption for different allowed CPAs for a site depth of 80 m and a hydrophone depth of 60 m. Additionally, the dashed line represents the same parameter for the nominal CPA distance of the deep water standard ISO 17208-1:2016 (2016) (100 m).

approximately 2.5 dB when comparing shallow water results with those from deep water. This article describes an improved method that reduces the observed underestimation: the SSCI method.

The SSCI method accounts for the measurement geometry (H, site depth; d_{CPA}, CPA distance; h_i, hydrophone depth; d_s, nominal source depth), and for the water and seabed parameters (c_w, sound speed in water; c_b, sound speed in seabed; ρ_w, mass density in water; ρ_b, mass density in seabed and β_b, seabed attenuation per wavelength). The method is summarized in Eqs. (16)–(25).

The precision and robustness of the SSCI were tested by comparing the results with numerical and analytical models, demonstrating that the method maintains the SCA accuracy at low frequencies while improving performance at high frequencies (>500 Hz).

The method's performance was also assessed based on test results, where ship SL measurements in shallow water were compared with measurements in deep water under the

same operational conditions as in deep water. For this real-case evaluation, numerous cases from the SATURN project tests were included, covering deployments with three hydrophones (VLAs and HLAs) and SHDs. In these scenarios, the average differences in the frequency range 150 Hz to 20 kHz for the VLA, HLA, and SHD deployments were −0.9, −1.3, and −1.5 dB, respectively. Furthermore, the standard deviation for the VLA and HLA deployments was similar (0.6 dB). In comparison, the SHDs exhibited a higher standard deviation (1.3 dB), confirming the prior expectation that the uncertainty associated with SHDs would be greater.

As an additional real-case evaluation, the SSCI method was applied to results from the MMP2 project, confirming the improvement and allowing for a more detailed exploration of performance at low frequencies (below 100 Hz), which was not possible with the results from the SATURN project (affected by flow noise from strong currents in the measurement area).

Additionally, a simplification of the method (SSCI-sim) is proposed, which reduces the complexity of the power reflection coefficient, requiring one less input parameter (the seabed attenuation per wavelength is not needed). This simplification is somewhat less accurate in soft substrates or at angles close to the critical angle (details provided in the supplementary material).

Furthermore, it is shown how the correction for water absorption (which becomes more significant from kilohertz frequencies) would have a notable impact within the accepted testing distance set by the draft standard ISO/DIS 17208-3 (2023) if levels are to be reported at frequencies exceeding 20 kHz, or at distances up to 5 times the site depth within the current bandwidth (10 Hz to 20 kHz). In both cases, water absorption should be considered.

A formula for the RNL metric in shallow water is also provided, as this term is particularly necessary since the draft standard returns results as SL and RNL and the initially described definition in ISO 17208-1:2016 (2016) only considers deep water.

SUPPLEMENTARY MATERIAL

See the supplementary material for a detailed derivation of the SSCI method, analysis of the simplification of the power reflection coefficient, and comparisons against the SCA method for different substrate types; for a spreadsheet file (Microsoft Excel format) providing a reference implementation of the SSCI PL formulas from Secs. II B and C; and for the SPLs (corrected for hydrophone sensitivity and background noise) from the SATURN project and corresponding metadata used to obtain reported SLs from Sec. V F.

ACKNOWLEDGMENTS

The work was funded by the EU Horizon 2020 Framework Programme research program SATURN (Developing Solutions to Underwater Radiated Noise, Grant No. 101006443). We acknowledge the contribution of two anonymous peer reviewers, whose helpful feedback improved the quality of the final manuscript.

AUTHOR DECLARATIONS

Conflict of interest

The authors have no conflicts to disclose.

DATA AVAILABILITY

The data that support the findings of this study are available within the article. The SATURN data used to derive SL results (Sec. V F) are available as supplementary material.

Ainslie, M. A. (**2010**). *Principles of Sonar Performance Modeling* (Springer, Berlin).

Ainslie, M. A., Bruliard, F.-A., de Jong, C. A. F., Díaz, J. A., Folegot, T., Ghasemi, M., Halvorsen, M. B., Slabbekoorn, H., Tougaard, J., and van der Schaar, M. (**2024a**). Deliverable D2.3: SATURN Acoustical Terminology Standard, Version 2.0. Technical report for SATURN.

Ainslie, M. A., MacGillivray, A. O., Yubero, R., de Jong, C. A. F., and Wang, L. S. (**2024b**). "Ship source measurement in shallow water using an enhanced seabed critical angle method," in *International Conference on Underwater Acoustics 2024*, Bath, UK (Institute of Acoustics, Milton Keynes, UK).

Ainslie, M. A., Martin, S. B., Trounce, K. B., Hannay, D. E., Eickmeier, J. M., Deveau, T. J., Lucke, K., MacGillivray, A. O., Nolet, V., and Borys, P. (**2022**). "International harmonization of procedures for measuring and analyzing of vessel underwater radiated noise," Mar. Pollut. Bull. **174**, 113124.

Ainslie, M. A., and Wood, M. A. (**2022**). "Semi-coherent image method to estimate propagation loss in shallow water for measuring surface vessel source level," Proc. Mtgs. Acoust. **47**, 070024.

Bahtiarian, M. A. (**2009**). "Standards: ASA standard goes underwater," Acoust. Today **5**(4), 30–33.

Blaeser, S., and Struck, C. J. (**2019**). "A history of ASA standards," J. Acoust. Soc. Am. **145**(1), 77–109.

EMODnet (**2024**). "EMODnet Map Viewer," https://emodnet.ec.europa.eu/geoviewer/ (Last viewed August 23, 2024).

Etter, P. C. (**2013**). *Underwater Acoustic Modeling and Simulation*, 4th ed. (CRC Press, Boca Raton, FL).

Hannay, D. E., Ainslie, M. A., Trounce, K. B., Eickmeier, J., MacGillivray, A. O., Martin, S. B., and Nolet, V. (**2023**). "Recommended Procedures for Measuring Underwater Radiated Noise Emissions of Ships, for Quiet Ship Certification," JASCO Document 03129, Version 2.0. Technical Report by JASCO Applied Sciences for Vancouver Fraser Port Authority (JASCO Applied Sciences, Victoria, Canada).

ISO 17208-1:2016 (**2016**). "Underwater acoustics—Quantities and procedures for description and measurement of underwater sound from ships—Part 1: Requirements for precision measurements in deep water used for comparison purposes" (International Organization for Standardization, Geneva, Switzerland), available at https://www.iso.org/standard/62408.html.

ISO 17208-2:2019 (**2019**). "Underwater acoustics—Quantities and procedures for description and measurement of underwater sound from ships—Part 2: Determination of source levels from deep water measurements" (International Organization for Standardization, Geneva, Switzerland), available at https://www.iso.org/standard/62409.html.

ISO 18405:2017 (**2017**). "Underwater acoustics—Terminology" (International Organization for Standardization, Geneva, Switzerland), available at https://www.iso.org/standard/62406.html.

ISO 80000-8:2020 (**2020**). "Quantities and units—Part 8: Acoustics" (International Organization for Standardization, Geneva, Switzerland), available at https://www.iso.org/standard/64978.html.

ISO/DIS 17208-3 (**2023**). "Underwater acoustics—Quantities and procedures for description and measurement of underwater sound from ships—Part 3: Requirements for measurements in shallow water" (International

Organization for Standardization, Geneva, Switzerland), available at https://www.iso.org/standard/81321.html.
ISO/TC 43/SC 3/WG 1 (**2011**). "Underwater acoustics," available at https://www.iso.org/committee/653046.html.
Jensen, F. B., Kuperman, W. A., Porter, M. B., and Schmidt, H. (**2011**). *Computational Ocean Acoustics* (Springer, New York), .
Lagrois, D., Martins, C. C. A., Sénécal, J.-F., Turgeon, S., and Chion, C. (**2024**). "Exploring the efficiency of a source-level model to predict hydrophone-based received noise levels of the St. Lawrence Estuary's merchant fleet," Ocean Eng. **309**, 118451.
MacGillivray, A. O., Martin, S. B., Ainslie, M. A., Dolman, J. N., Li, Z., and Warner, G. A. (**2023**). "Measuring vessel underwater radiated noise in shallow water," J. Acoust. Soc. Am. **153**(3), 1506–1524.
MacGillivray, A. O., Martin, S. B., Ainslie, M. A., Dolman, J. N., Li, Z., Warner, G. A., Lawrence, C. B., Pace, F., Schuster, M., and Wittekind, D. (**2022**). "Towards a Standard for Vessel URN Measurement in Shallow Water: Final Report on Transport Canada Innovation Centre Project MMP2" (JASCO Applied Sciences, Victoria, Canada).
SATURN (**2020**). "Developing solutions to underwater radiated noise," available at https://www.saturnh2020.eu/ (Last viewed September 5, 2024).
Schmidt, H. (**2004**). OASES Version 3.1 User Guide and Reference Manual, Department of Ocean Engineering, Massachusetts Institute of Technology, Cambridge, MA.
Schmidt, H., and Jensen, F. B. (**1985**). "A full wave solution for propagation in multilayered viscoelastic media with application to Gaussian beam reflection at fluid–solid interfaces," J. Acoust. Soc. Am. **77**(3), 813–825.
Wang, L., Heaney, K., Pangerc, T., Theobald, P., Robinson, S., and Ainslie, M. A. (**2014**). "Review of Underwater Acoustic Propagation Models," NPL Report No. AC 12 (National Physical Laboratory, Teddington, UK).
Yubero, R., Ghasemi, M., and Solheim Pettersen, Ø. (**2023**). "Deliverable D2.1: Final Report on Vessel URN Measurements," Version 1.0. Technical Report for SATURN, available at https://cordis.europa.eu/project/id/101006443/results.